THE BINARY FRACTION OF LOW MASS WHITE DWARFS

Justin M. Brown
Franklin and Marshall College
415 Harrisburg Avenue, Lancaster, PA 17604 USA

Mukremin Kilic, Warren R. Brown, and Scott J. Kenyon
Smithsonian Astrophysical Observatory
60 Garden Street, Cambridge, MA 02138 USA
Draft version January 28, 2011

ABSTRACT

We describe spectroscopic observations of 21 low-mass ($\leq$0.45 M$_\odot$) white dwarfs (WDs) from the Palomar-Green Survey obtained over four years. We use both radial velocities and infrared photometry to identify binary systems, and find that the fraction of single, low-mass WDs is $\leq$30%. We discuss the potential formation channels for these single stars including binary mergers of lower-mass objects. However, binary mergers are not likely to explain the observed number of single low-mass WDs. Thus additional formation channels, such as enhanced mass loss due to winds or interactions with substellar companions, are likely.

Subject headings: White Dwarfs — stars: Low-Mass — stars: Evolution

1. INTRODUCTION

Around 10% of white dwarfs (WDs) in the solar neighborhood are low-mass ($M < 0.45$ M$_\odot$) helium-core objects (Liebert et al. 2005). The oldest globular clusters in the Galactic halo are currently producing $\approx$0.53 M$_\odot$ WDs (Kalirai et al. 2009). Hence, the presence of low-mass helium-core WDs in the Galactic disk requires a formation mechanism other than the normal single star evolution. The most commonly accepted formation channel for low-mass WDs is through enhanced mass loss from post-main-sequence stars in interacting binary systems. Such stars can lose their outer envelopes without reaching the asymptotic giant branch and without ever igniting helium, thus ending up as helium-core WDs. The large number of low-mass WDs found in binary systems support this formation scenario (Rebassa-Mansergas et al. 2011). However, not all low-mass WDs are found in binary systems (Marsh et al. 1995; Maxted et al. 2000; Napiwotzki et al. 2004).

Nelemans & Tauris (1998) propose a scenario for the formation of single low-mass WDs in which binary interactions of post-main-sequence stars with close-in massive planets can expel the stellar envelope. The planets may or may not survive the common envelope evolution. In the latter case, there is no way of knowing whether low-mass WDs are produced through this formation channel. Nelemans & Tauris (1998) predict that the minimum companion mass required to expel the envelope of the progenitor 1 M$_\odot$ star is 21 M_J. Based on mid-infrared photometry, Kilic et al. (2010) limit any undetected companions to $M < 40 M_J$ around eight single low-mass WD systems. Therefore, a well tuned common-envelope phase scenario involving 20-40 M_J companions is required to explain the radial velocity and infrared observations of the apparently single low-mass WDs. Even though this scenario seems unlikely, it cannot be ruled out due to the caveats in our understanding of the common-envelope phase evolution.

An alternative scenario for the formation of single low-mass WDs was proposed by Hansen (2005) to explain the color-magnitude distribution of the WDs in the metal-rich cluster NGC 6791. Metal-rich stars have increased opacities and thus increased mass loss winds; extrapolating theoretical mass loss models to [Fe/H]=+0.4 suggests that mass loss can approach 0.4–0.5 M$_\odot$ on the red giant branch (Catelan 2000). Thus a single low-mass WD may result from a single metal-rich star because of severe mass loss winds on the red giant branch. Kalirai et al. (2007) observe that most of the brightest WDs in NGC 6791 are indeed low-mass WDs, and they suggest that at least 40% of the stars in that cluster have lost enough mass on the red giant branch to end up as He-core WDs. The relatively large fraction of low-mass WDs in NGC 6791 compared to the 10% fraction in the field WD sample likely points to the dependency of stellar evolution on metallicity. Thus a mechanism exists to produce single low-mass WDs in metal-rich environments.

In the mass-loss wind scenario, the formation rate of single $\sim$0.4 helium WDs is dominated by the old stellar population; intermediate-mass metal-rich stars, even with enhanced mass loss winds, have enough mass to ignite helium in their cores and eventually form ordinary carbon-oxygen WDs. According to the Reid et al. (2007) analysis of stars within 30 pc, 3% of solar neighborhood stars with >8 Gyr ages have [Fe/H]>+0.3. This is comparable to the fraction of single low-mass WDs in the PG survey WD population, which Kilic et al. (2007) estimate is 4%. Thus single metal-rich field stars provide another possible origin for single low-mass WDs.

All three scenarios mentioned above – mass-loss due to binary companions, planets, and winds – likely contribute to the population of low-mass WDs, the question is by how much. The binary formation channel is generally considered to be the dominant mechanism, however the remaining two channels are also likely to contribute.

brown.justin.michael@gmail.com
mkilic, wbrown, skenyon@cfa.harvard.edu

TABLE 1
PHYSICAL PARAMETERS

Object	M (M$_\odot$)	T_{eff} (K)	V (mag)	J (mag)
PG 0132+254	0.41	19960	16.12	16.446 ± 0.127
PG 0237+242	0.40	69160	16.71	16.278 ± 0.102
PG 0808+595	0.42	27330	16.01	16.608 ± 0.125
PG 0834+501	0.40	60350	15.24	16.085 ± 0.104
PG 0846+249	0.40	66110	16.71	17.520 ± 0.093*
PG 0934+338	0.38	24380	16.35	16.569 ± 0.150
PG 0943+441	0.41	12820	13.29	13.643 ± 0.025
PG 1022+050	0.44	11680	14.20	14.228 ± 0.129*
PG 1036+086	0.42	22230	16.26	16.895 ± 0.055*
PG 1101+364	0.32	13040	14.49	14.821 ± 0.041*
PG 1114+224	0.41	25860	16.32	16.970 ± 0.106*
PG 1202+608	0.40	58280	13.60	14.359 ± 0.032
PG 1210+141	0.34	31930	14.71	15.316 ± 0.035
PG 1224+309	0.42	28820	16.15	15.080 ± 0.040*
PG 1229−013	0.41	19430	13.79	14.925 ± 0.029
PG 1241−010	0.40	23800	14.00	14.419 ± 0.043
PG 1249+160	0.39	25590	14.62	15.219 ± 0.043
PG 1252+378	0.36	79900	15.77	15.738 ± 0.063
PG 1317+453	0.36	13320	14.14	14.317 ± 0.034
PG 1320+645	0.44	27130	16.38	17.099 ± 0.079*
PG 1415+133	0.42	34270	15.37	14.263 ± 0.034
PG 1458+172	0.41	21950	16.30	14.701 ± 0.029
PG 1519+500	0.42	28730	16.45	16.950 ± 0.097*
PG 1554+262	0.45	21220	16.87	17.011 ± 0.083*
PG 1614+136	0.40	22430	15.24	15.704 ± 0.058
PG 1654+637	0.44	15070	15.65	16.167 ± 0.102
PG 1713+333	0.41	22120	14.49	14.900 ± 0.031
PG 2226+061	0.44	15280	14.71	15.178 ± 0.044
PG 2257+162	0.43	24580	16.14	15.439 ± 0.053
PG 2331+290	0.44	27320	15.85	16.177 ± 0.090

NOTE. — M, T_{eff}, and V are from Liebert et al. (2005); J is from Cutri et al. (2003), except for those objects (*) with our own photometry.

Understanding the frequency of binary/single low-mass WDs is necessary to constrain the formation models.

In this paper, we measure the binary frequency of the 30 low-mass WDs found in the Palomar Green (PG) Survey (Green et al. 1986). We provide 720 radial velocity observations for the 21 previously unstudied low-mass WDs, and investigate the near-infrared color excess of the whole sample. We find that at least 70% of the PG WDs with ≤ 0.45 $M_\odot$ are binaries, and compare this observed binary fraction and orbital period distribution to other samples of WDs and to low-mass WD formation models.

2. OBSERVATIONS AND TECHNIQUES

Our sample of thirty ≤ 0.45 $M_\odot$ low-mass WDs is taken from the PG Survey, a comprehensive survey of blue stellar objects with $B \lesssim 16.1$ (Green et al. 1986). The PG Survey covers 10,714 square degrees with an estimated completeness of 84%. Liebert et al. (2005) fit stellar atmosphere models to the 348 DA WDs in the PG survey and identify 30 WDs with mass less than 0.45 $M_\odot$. This is the sample of WDs studied here. The mass and effective temperature determined by Liebert et al. (2005) are listed in Table 1.

2.1. Photometry

We take V-band photometry from Liebert et al. (2005) and near-infrared photometry from the Two Micron All Sky Survey (2MASS) (Cutri et al. 2003). In addition, for nine objects we obtain deeper near-infrared photometry

using the Peters Automated Infrared Imaging Telescope (PAIRITEL) – the old 2MASS north telescope operated with the original 2MASS camera (Bloom et al. 2006). The photometry of the 30 low-mass WDs is tabulated in Table 1.

2.2. Spectroscopy

We obtain spectroscopy for the 21 low-mass WDs with no previously known radial velocity variability. The other 9 WDs are known binary systems published elsewhere (Marsh et al. 1995; Marsh 1995; Holberg et al. 1995; Orosz et al. 1999; Morales-Rueda et al. 2005; Nelemans et al. 2005). To verify our data reduction and analysis procedures, we re-observed one of the known binaries, PG 2331+290, and confirmed its 4 hr orbital period.

We obtained 720 spectra between October 2007 and April 2010 using the FAST spectrograph (Fabricant et al. 1998) on the Fred Lawrence Whipple Observatory 1.5m telescope. The spectrograph was operated with a 1.5″ slit and a 600 line mm^{-1} diffraction grating. This spectrograph set-up provides a wavelength range of 3500 to 5500 Å at a spectral resolution of 1.7 Å. All observations were obtained with a comparison lamp exposure following the science target exposure.

We process the spectra using IRAF[1] following the guidelines in Massey (1997). We determine radial velocities using the cross-correlation package RVSAO (Kurtz & Mink 1998) with the following procedure. First, we measure preliminary velocities by cross-correlating with a high signal-to-noise WD template of known velocity. Second, we shift each object's spectra to rest frame and sum them together to create a high signal-to-noise template of each object. Finally, we cross-correlate the individual spectra with their respective template to obtain radial velocities with the highest possible precision. The average uncertainty of our radial velocities is ±16 km s^{-1}.

We verify the accuracy of our velocities by measuring two night sky emission lines, Hg 4358.335 Å and 5460.750 Å. We find that the night sky lines have a 0 km s^{-1} mean and a 10 km s^{-1} dispersion in the data obtained in 2009 and 2010. However, the night sky lines exhibit a larger dispersion and non-zero means up to ~10 km s^{-1} in the data obtained prior to 2009. We account for this systematic error by adding ±10 km s^{-1} in quadrature to the radial velocity errors for spectra obtained prior to 2009.

3. RESULTS

We identify binary systems among our low-mass WD sample in two ways: by radial velocity variability, and by infrared color excess. We cannot detect all binary companions, of course. Radial velocity variability is sensitive to companions of any type, but only for small orbital separations and non-zero inclinations. Infrared photometry is sensitive to companions of any orbital separation and inclination, but only for main sequence (M dwarf)

---

[1] IRAF is distributed by the National Optical Astronomy Observatories, which are operated by the Association of Universities for Research in Astronomy, Inc., under cooperative agreement with the National Science Foundation.

stars that produce a significant infrared color excess. Despite these limitations we find that at least 70% of our WDs have binary companions, and for these systems we estimate the mass and nature of the companions.

3.1. Spectroscopic Binaries

We begin by fitting orbits to our radial velocity data, and then testing whether the observed velocity variability is statistically significant. We search for orbital periods in our radial velocity data using a Lomb periodogram (Press 1994). Period aliases are present for all of our WDs, thus we select the period that minimizes χ^2 for a circular orbital fit following Kenyon & Garcia (1986). Figure 1 (see also Figure 3) plots the radial velocities phased to the best-fit periods for the objects with well-determined orbits.

We use an F-test to calculate the significance level at which the orbital fits have a smaller variance than a constant velocity fit. For a significance threshold of 0.01, we find 7 WDs with significant orbital fits. The orbital elements for the 7 WDs are presented in Table 5. As discussed in Brown et al. (2010), uncertainties in the orbital elements are derived from the covariance matrix and χ^2.

Curiously, of the WDs for which we cannot fit orbits, two objects (PG 0846+249 and PG 1320+645) have significant velocity variability (listed in Table 5 as having "high dispersion"). Although we require more data to constrain a period for these two WDs, we consider them probable binary systems.

Table 5 summarizes the orbital properties for the entire sample of 30 low-mass WDs. For our 7 newly discovered binaries, we present the orbital period P, velocity semi-amplitude K, systemic velocity γ, time of spectroscopic conjunction T_0, the F-test significance, the mass function MF, the minimum companion mass M_2, and the maximum merger time τ. For the 14 WDs with no orbital fit, we present the systemic velocities and, in place of the semi-amplitude, the standard deviation of the velocities. Finally, for the 9 previously known binaries, we present the published periods and mass functions as noted in Table 5.

3.1.1. Orbital Properties

Sixteen of the 30 low-mass WDs in our sample (7 from our observations and 9 from the literature) are binaries with well-measured orbits. For these systems we calculate the companion masses, merger times, and likelihood to produce Type Ia supernovae ($M_{tot} \geq 1.4$ M$_\odot$).

The orbital mass function relates the observed period P and velocity semi-amplitude K to the mass of the two components, M_1 and M_2, and the inclination i:

$$\frac{PK^3}{2\pi G} = \frac{(M_2 \sin i)^3}{(M_1 + M_2)^2}. \quad (1)$$

Because the mass of the WD, M_1, is known from stellar atmosphere model fits (Liebert et al. 2005), we can use the mass function to solve for the mass of the unseen companion, $M_2 \sin i$. An edge-on orbit with $i = 90°$ gives the minimum possible companion mass and is presented in Table 5.

Our WD binaries are potential candidates for mergers. A short-period binary loses energy through gravitational
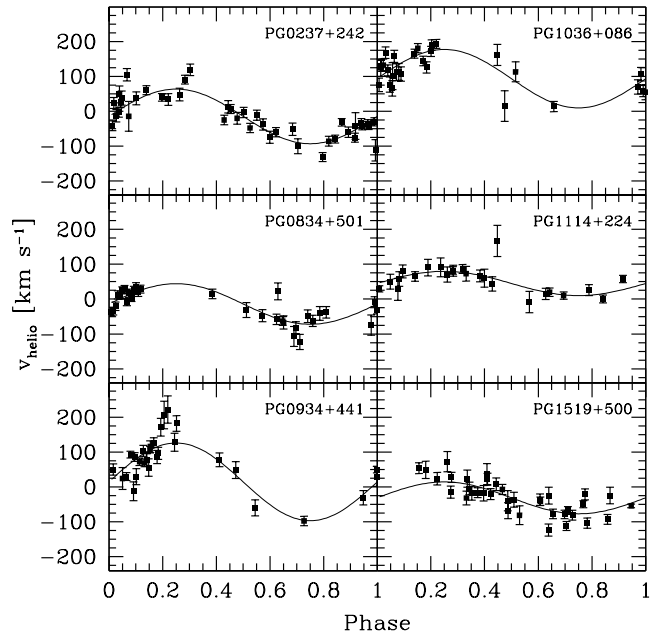

FIG. 1.— Radial velocities for 6 WDs with well-determined orbits, phased to the best-fit periods (see Table 5).

wave radiation, leading to an inward spiral of the objects until they merge (Postnov & Yungelson 2005). We calculate the merger times following Landau & Lifshitz (1958),

$$\tau = \frac{(M_1 + M_2)^{\frac{1}{3}}}{M_1 M_2} P^{\frac{8}{3}} \times 10^{-2} \text{ Gyr}, \quad (2)$$

where the masses are in $M_\odot$, and the period is in hours. We use the minimum companion masses to calculate the maximum possible merger times, presented in Table 5.

Two of the WD+WD binaries, PG 1101+364 and PG 2331+290, will merge within a Hubble time. If the combined mass of the system exceeds the Chandrasekhar limit, the merger may result in a Type Ia Supernova. The cumulative probability function of orbital inclination for a random stellar sample is $1 - \cos i$ (Imbert & Prevot 1998). Using this relation, we calculate the probability of the merging binary systems becoming Type Ia Supernovae. None of these systems have probabilities greater than 2% of becoming Type Ia Supernovae. Two additional systems in our survey, PG 1224+309 and PG 1458+172 (discussed below) are WD+MS binaries with merger times shorter than a Hubble time. These two systems will evolve into cataclysmic binaries within several Gyr.

3.2. Photometric Binaries

We now use infrared photometry to search for binary companions to the low mass WDs. We begin by comparing the observed $(V-J)$ color of each WD with the expected $(V-J)$ color from the models of Bergeron et al. (1995) for the appropriate WD mass and effective temperature. If there is a $(V-J)$ color excess with more than 2σ significance, we classify the WD as having a probable (M-dwarf) companion.
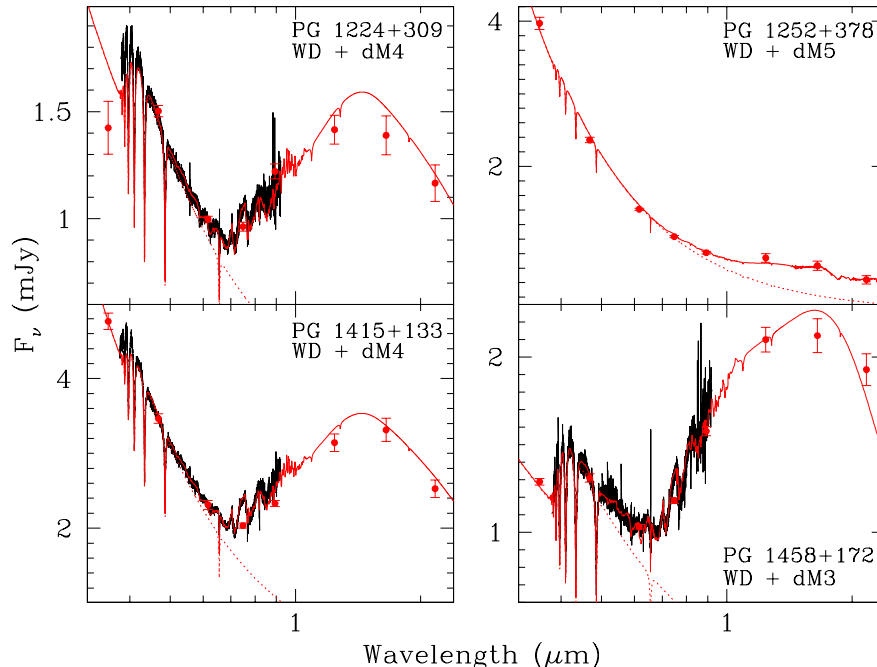
Fig. 2.— The spectral energy distributions for four WDs with infrared excess. SDSS and 2MASS photometry are plotted with red dots. Spectroscopy is drawn in black. The best-fit WD (dashed red line) plus M dwarf model is drawn with the solid red line.

Five of the 30 WDs have significant infrared color excess, and are listed in Table 2. A sixth WD (PG 0237+242) with possible color excess was shown by Kilic et al. (2010) to have no mid-infrared signature of a companion. Kilic et al. (2010) also studied PG 2257+162, one of our five WDs with color excess, and found clear evidence for a 3300 K ($\approx$ M4 spectral type) companion in the mid-infrared *Spitzer* photometry.

Figure 2 plots the spectral energy distribution for the other four WDs with color excess. All four objects also have *ugriz* photometry available from the Sloan Digital Sky Survey. In Figure 2 we compare the optical and near-infrared photometry (points) to the observed SDSS spectra (black line) and to theoretical WD plus M-dwarf models (red lines). All four WDs are well modeled with main sequence M-dwarf companions with spectral types M3-M5 (Pickles 1998). Based on known M3-M5 dwarfs in eclipsing binaries, we estimate that M3, M4, and M5 dwarfs have masses of 0.28, 0.22, and 0.19 $M_\odot$, respectively (Çakırlı & Ibanoğlu 2010; Irwin et al. 2010; Morales et al. 2009). The formal precision of these mass estimates is ± 0.05 $M_\odot$.

3.3. *Comparison of Photometry and Spectroscopy*

Knowing the masses and the velocity amplitude (or limits to the velocity amplitude) of the binary systems, we can place limits on the orbital periods and inclinations using the mass function (Equation 1). We separate period and inclination by assuming, for purposes of discussion, the mean inclination angle of a random stellar sample, $i = 60°$, and the mean orbital period observed in our sample, $P \simeq 1$ day. Table 2 summarizes the results. The columns in Table 2 are $M_{2,\mathrm{phot}}$, the photometric mass estimate, $P_{\mathrm{For}\ i=60°}$, the orbital period given the observed velocity amplitude and a $60°$ inclination, and

TABLE 3
PHOTOMETRIC BINARIES

Object	$M_{2,\mathrm{phot}}$ ($M_\odot$)	$P_{\mathrm{For}\ i=60°}$ (days)	$i_{\mathrm{For}\ \mathrm{P=1day}}$ (°)
PG 1224+309	0.22	$\cdots$	$\cdots$
PG 1252+378	0.19	5.3	30°
PG 1415+133	0.22	20.4	18°
PG 1458+172	0.28	$\cdots$	$\cdots$
PG 2257+162	0.22	8.0	26°

$i_{\mathrm{For}\ \mathrm{P=1day}}$, the orbital inclination given the observed velocity amplitude and a 1 day period.

Three systems with color excess have no detected radial velocity variability. The implied orbital parameters for these three systems, given the photometric companion mass estimates, are consistent with the radial velocity observations. Given the 20–30 km s^{-1} upper limits to the velocity semi-amplitudes, PG 1252+378, PG 1415+133, and PG 2257+162 could be binaries with either week-long orbital periods (assuming $i = 60°$) or relatively pole-on $i < 30°$ inclinations (assuming $P=1$ day). We would not detect any of these systems with our radial velocity data.

Two systems with color excess, PG 1224+309 and PG 1458+172, have significant radial velocity variability. Both systems show hydrogen and magnesium emission lines from the irradiated face of the secondary star. Orosz et al. (1999) used radial velocity observations of PG 1224+309 to constrain the mass of the companion to 0.28 ± 0.05 $M_\odot$. This mass estimate is consistent with our photometric mass estimate within the errors. Given the 6.2 hr period of this binary system, PG 1224+309 will evolve into a cataclysmic variable system within a Hubble time.
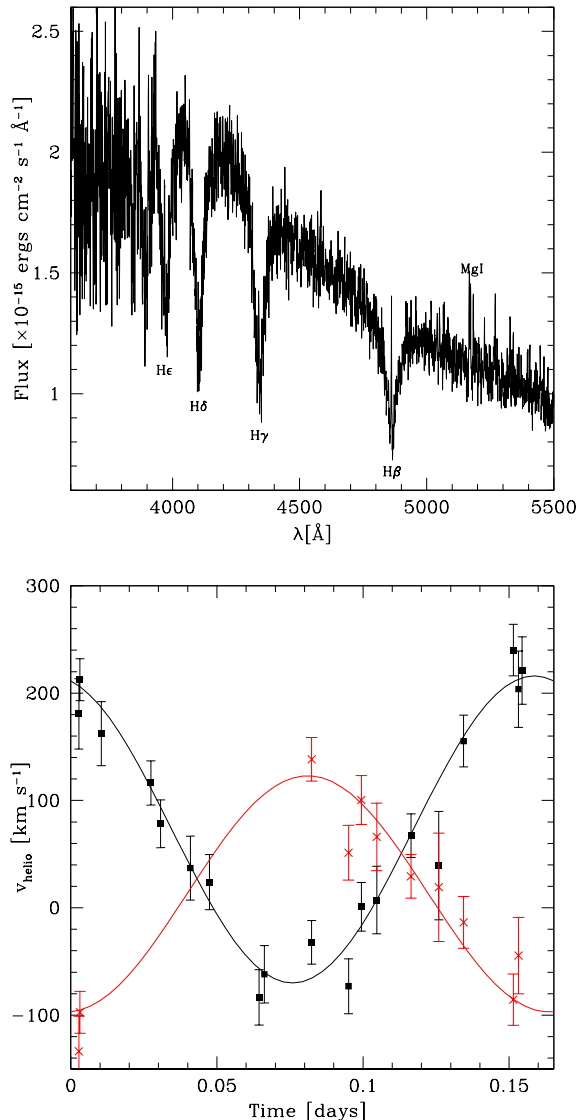
FIG. 3.— (*Top*) Typical PG 1458+172 spectrum, unsmoothed, with H and Mg lines seen in emission. (*Bottom*) Observations phased to the best-fit 3.968 hr period for both absorption line velocities (squares) and emission line velocities (x's).

3.4. *PG 1458+172*

PG 1458+172 is a new pre-cataclysmic binary discovered in our survey. The optical spectrum of this object shows Balmer lines both in absorption and emission and a Mg I triplet (λ 5167.321 Å , 5172.684 Å , and 5183.604 Å) in emission as seen in Figure 3. Strong Hα emission is also evident in the SDSS spectroscopy. The radial velocity variation of the emission lines is about $190°$ out of phase with the Balmer absorption lines from the WD primary. We use the H and Mg emission lines to fit an independent orbit to the secondary, and list the orbital parameters in Table 5 under PG 1458 (Mg). Both the primary and secondary have best-fit periods of 0.16532 ± 0.00033 days.

The ratio of the velocity amplitudes, combined with the 0.41 $M_\odot$ WD mass from (Liebert et al. 2005), suggests that the secondary has a mass of 0.55 $M_\odot$. How-

ever, the center of light of the emission features is different than the center of mass of the companion. If the emission features come from the heated face of the companion, for example, we would expect a shift in the velocity semi-amplitude of the emission features (Orosz et al. 1999). Fortunately, we detect the light of the companion in the infrared (see Figure 2) which provides a more reliable companion mass estimate.

Figure 2 shows that the infrared excess around PG 1458+172 is consistent with an M3 (0.28 $M_\odot$) dwarf companion. This is significantly lower than predicted by the mass function and the spectroscopic mass measurement for the WD. Liebert et al. (2005), unaware of the Balmer emission features, likely over-estimated the WD mass, however. Higher signal-to-noise ratio spectroscopy covering the Hα emission line is needed to properly characterize the orbits and masses of the individual components in this pre-cataclysmic binary.

3.5. *Binary Fraction and Completeness*

Of the 21 low-mass WDs we observed from the Palomar-Green Survey, seven of these have clear periodic radial velocities, two have large enough dispersion to be binary systems (without our being able to constrain a period), and three of those without strong velocity variation have infrared excess, indicating a companion. Including the nine objects from the literature that comprise the 30 low-mass WD sample of the Palomar-Green Survey, 21 show significant evidence for a companion. Thus the binary fraction of our $\simeq$0.4 $M_\odot$ WDs is at least 70%.

Some binaries must escape our detection, however. We are not sensitive to binary systems with intrinsically faint companions (such as brown dwarfs and WDs) that have pole-on orientations, or large orbital separations. For a sample of 30 binary systems with random orbital inclinations, there should be 4 pole-on systems with $i < 30°$ for which we would not detect radial velocity variability. Given our discovery rates, one of these hypothetical pole-on systems should be identified by infrared photometry. Thus there may be an additional 3 (10%) more binaries in our sample, undetected because they are pole-on systems. Put another way, $20\% - 30\%$ of our low-mass WDs may exist in single systems.

Additional observations suggest that some of the low-mass WDs are indeed single. Maxted et al. (2000) have 7-15 radial velocity measurements for five of the possible single systems (PG 0132+254, 0808+595, 1229−013, 1614+136, and 2226+061) and do not detect significant radial velocity variations for any of these objects. Equally important, mid-infrared photometry by Kilic et al. (2010) rules out the presence of both stellar and massive brown dwarf companions in six of the apparently single systems in our sample. We conclude that possibly six (20%), but no more than nine (30%), of our 30 targets are single low-mass WDs.

4. DISCUSSION

4.1. *Comparison to Population Synthesis Models*

The observed fraction of WD binary systems is related to WD mass. WDs with 0.5-0.7 $M_\odot$ and 0.7-1.1 $M_\odot$ observed in the volume-limited sample of Holberg et al. (2008) have binary fractions of at least 32% and 6%, respectively. The binary fraction of extremely low-mass
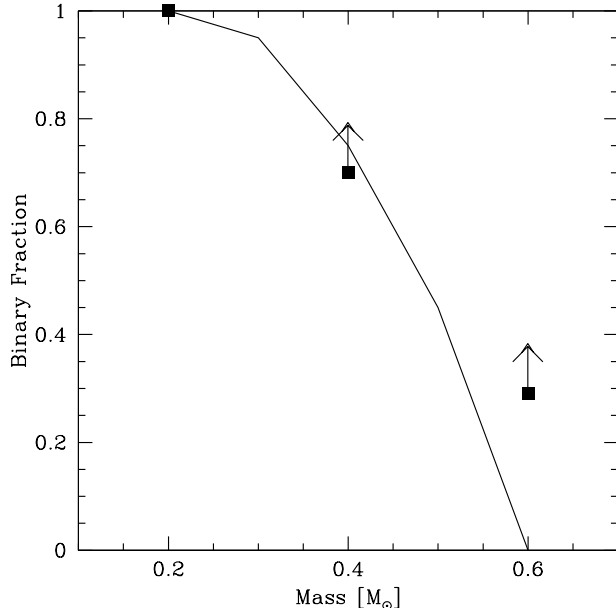
Fig. 4.— The observed binary fractions of WDs as a function of mass, compared to a theoretical binary evolution model (Nelemans 2010, private communication). The 0.2 $M_\odot$ WDs are from Brown et al. (2010), the 0.4 $M_\odot$ WDs are from this paper, and the 0.6 $M_\odot$ WDs are from Holberg et al. (2008).

WDs with $\leq$ 0.25 M$_\odot$, on the other hand, is 100% (Brown et al. 2010; Kilic et al. 2011). Hence, the binary fraction of WDs rises as the WD mass falls. In principle, we can use this relation between binary fraction and WD mass to constrain binary evolution models.

Nelemans & Tout (2005) perform population synthesis calculations for single and double WD systems. The predicted WD binary fraction depends on at least three factors: the physics of common envelope phase evolution and the initial mass distribution and orbital period distribution of the progenitor binaries. In these models, for example, a portion of the single low-mass WD population forms from He+He WD mergers (Nelemans 2010).

Figure 4 compares the result of the Nelemans et al. population synthesis models with the observations. The models predict binary fractions of 100% and 75% for 0.2 and 0.4 M$_\odot$ WDs, respectively. The observed binary fractions agree remarkably well with model predictions for low-mass WDs. Given the uncertainties in the population synthesis calculations, however, it is worth comparing the observed binary fraction of low-mass WDs with that of single subdwarf stars.

The majority (90%) of He+He WD mergers are expected to create subdwarf B stars, the mass of which are expected to exceed the helium ignition limit of $\approx$ 0.45 M$_\odot$. The birth rate of single subdwarf B stars is 2×10^{-14} pc^{-3} yr^{-1} (Nelemans 2010). In comparison, the formation rate of 0.4 M$_\odot$ WDs in the PG survey is $\sim 4 \times 10^{-14}$ pc^{-3} yr^{-1} (Liebert et al. 2005). Thus the formation rate of single low-mass WDs, given our observations, is $\sim 10^{-14}$ pc^{-3} yr^{-1}. This is comparable to the birth rate of single subdwarf B stars, which means that the merger scenario by itself cannot explain the formation rate of single low-mass WDs.

Nelemans & Tauris (1998) discuss the possibility of

creating single low-mass WDs through common envelope evolution of solar mass stars with massive planets or brown dwarfs in close (< 3 yrs) orbits. However, the absence of stellar or massive brown dwarf ($\geq 40 M_J$) companions to half a dozen apparently single low-mass WDs restricts the potential companions to a narrow mass range, where they are massive enough to expel the stellar envelope during the common envelope phase but also small enough to avoid detection in the mid-infrared (Kilic et al. 2010). A well tuned scenario involving a common envelope phase between a 1 M$_\odot$ star and a 20-40 M_J brown dwarf at a certain orbital separation can explain the single low-mass WDs, but it seems unlikely that this scenario will explain all single low-mass WDs.

Kilic et al. (2007) propose that a significant fraction of nearby field stars have super-solar metallicity and that the single low-mass WD population can form through enhanced mass loss from these stars. We find up to 9 single low-mass WDs from the 348 DA WDs in the PG survey, or 2.6%. Similarly, Nelemans (2010) find that 15 of 636 WDs (2.4%) observed in the SPY survey are single low-mass WDs. Kilic et al. (2007) estimate that the fraction of metal-rich stars with [Fe/H] > +0.3 has been more than 2-3% in the past 10 Gyr. Thus the observed frequency of single low-mass WDs is consistent with the enhanced mass-loss scenario.

While binary frequency provides a useful constraint on formation scenarios, the period distribution is fundamental to evolution of the low-mass WD binary systems. Figure 5 compares the observed orbital period distribution of two complete, magnitude-limited samples: the 0.4 M$_\odot$ WDs studied here, and the 0.2 M$_\odot$ WD systems studied by Brown et al. (2010). Interestingly, none of the 0.2 M$_\odot$ WD systems have orbital periods longer than a day, whereas at least 40% the 0.4 M$_\odot$ WD systems have orbital periods longer than a day. The tightest main-sequence binary systems will interact the earliest in their evolution; they will go through common envelope phases, lose their envelopes before helium ignition in the core, and end up as He-core WDs in even tighter binary systems. Thus finding the lowest mass WD binaries in the most compact binary systems is consistent with our understanding of binary evolution.

4.2. Implications

We close by noting that old, metal-rich stellar populations dominate in many astrophysical environments, namely, the bulges and spheroids of galaxies. The existence of single low-mass WDs in the field, as well as the observed stellar population of NGC 6791, demonstrate that old, metal-rich stars are evolving through at least one of the unique channels discussed here. These evolution channels will affect the red giant luminosity function, blue horizontal branch morphology, and the integrated light of the overall stellar population (Kalirai et al. 2007). Han et al. (2010), for example, argue that hot subdwarf stars formed from He-He WD mergers naturally explain the UV-upturn seen in the integrated light of elliptical galaxies. Thus the existence of single low-mass WDs in the field, and the evolutionary channels they are linked to, has important implications for interpreting the age, metallicity, and mass-to-light ratio of metal-rich stellar populations throughout the Universe.
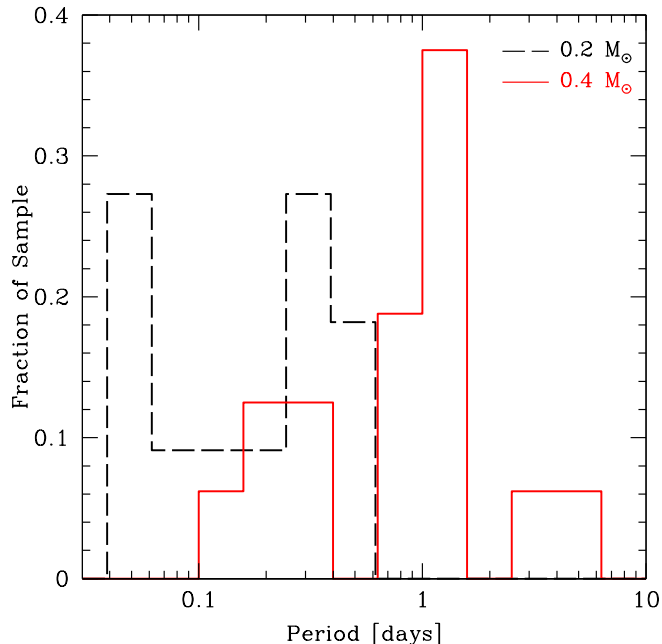
FIG. 5.— The period distribution of our magnitude-limited sample of 0.4 M$_\odot$ WDs (solid histogram) compared to the magnitude-limited sample of 0.2 M$_\odot$ WDs from Brown et al. (2010) (dashed histogram).

5. CONCLUSIONS

We discuss radial velocity and photometric observations of 30 low-mass WDs identified in the magnitude limited PG survey. We identify a total of 21 binary systems and provide orbital parameters and limits on companion masses. Our sample includes two WD+WD merger systems and two pre-cataclysmic binaries, one of which is a new discovery.

Nine objects in our survey do not show significant radial velocity variations. Six of these objects have mid-infrared photometry and none show mid-infrared excess from stellar or massive brown dwarf companions. Thus the fraction of single, low-mass WDs is 20%–30%. We discuss the potential formation channels for these single low-mass WDs: binary mergers of lower-mass objects, mass loss due to interactions with substellar companions, and mass loss due to super-solar metallicity winds. Binary mergers of two lower-mass WDs would most likely create He-burning sdB stars more massive than 0.4 M$_\odot$. The birth rates of single subdwarf B and low-mass WD stars are comparable. Therefore, the merger scenario is unlikely to explain all of the single low-mass WDs. Instead, a significant fraction of the single low-mass WDs may form as a result of interactions on the red giant branch with substellar companions or because of enhanced mass loss from the most metal-rich stars in the solar neighborhood.

Our understanding of the different formation channels for single low-mass WDs will benefit from infrared observations that can put strong limits on potential substellar companions and from theoretical studies on common envelope evolution and the fate of short period MS + brown dwarf (or massive planet) systems. The observed mass and period distributions of our targets are useful for constraining binary evolution theory via population synthesis studies, which can probe different evolutionary channels for low-mass WD formation.

APPENDIX

RADIAL VELOCITY DATA

Table 4 presents our 720 radial velocity measurements for 21 low-mass WDs. We also present 11 emission line velocity measurements, labeled PG 1458(Mg). The table columns are: (1) Object name, (2) heliocentric Julian date, and (3) heliocentric radial velocity. Table 4 is available in its entirety in machine-readable form in the online journal. A portion of the table is shown here for guidance regarding its form and content.

REFERENCES

Bergeron, P., Wesemael, F., & Beauchamp, A. 1995, PASP, 107, 1047
Bloom, J. S., Starr, D. L., Blake, C. H., Skrutskie, M. F., & Falco, E. E. 2006, in ASP Conf. Ser., Vol. 351, ADASS XV, ed. C. Gabriel, C. Arviset, D. Ponz, & S. Enrique, 751
Brown, W. R., Kilic, M., Allende Prieto, C., & Kenyon, S. J. 2010, ApJ, 723, 1072
Çakırlı, Ö. & Ibanoğlu, C. 2010, MNRAS, 401, 1141
Catelan, M. 2000, ApJ, 531, 826
Cutri, R. M. et al. 2003, 2MASS All Sky Catalog of point sources. (IPAC)
Fabricant, D., Cheimets, P., Caldwell, N., & Geary, J. 1998, PASP, 110, 79
Green, R. F., Schmidt, M., & Liebert, J. 1986, ApJS, 61, 305

Han, Z., Podsiadlowski, P., & Lynas-Gray, A. 2010, Ap&SS, 329, 41
Hansen, B. M. S. 2005, ApJ, 635, 522
Holberg, J. B., Saffer, R. A., Tweedy, R. W., & Barstow, M. A. 1995, ApJ, 452, L133+
Holberg, J. B., Sion, E. M., Oswalt, T., McCook, G. P., Foran, S., & Subasavage, J. P. 2008, AJ, 135, 1225
Imbert, M. & Prevot, L. 1998, A&A, 334, L37
Irwin, J. et al. 2010, ApJ, 718, 1353
Kalirai, J. S., Bergeron, P., Hansen, B. M. S., Kelson, D. D., Reitzel, D. B., Rich, R. M., & Richer, H. B. 2007, ApJ, 671, 748
Kalirai, J. S., Saul Davis, D., Richer, H. B., Bergeron, P., Catelan, M., Hansen, B. M. S., & Rich, R. M. 2009, ApJ, 705, 408
Kenyon, S. J. & Garcia, M. R. 1986, AJ, 91, 125

8

TABLE 4
RADIAL VELOCITY MEASUREMENTS

Object	HJD+2450000 (days)	v_{helio} (km s^{-1})
PG 0132+254	4385.783721	38.7 ± 14.2
$\cdots$	4385.834625	-6.3 ± 15.5
$\cdots$	4385.871130	-18.4 ± 13.0
$\cdots$	4385.884278	53.3 ± 15.2
$\cdots$	4385.909800	12.3 ± 13.3

NOTE. — Table 4 is presented in its entirety in the electronic edition of the Astrophysical Journal. A portion is shown here for guidance and content. NOTE: The complete "data.table" is also included in the arXive source file.

8

Kilic, M., Brown, W. R., Allende Prieto, C., Agüeros, M. A., Heinke, C., & Kenyon, S. J. 2011, ApJ, 727, 3

Kilic, M., Brown, W. R., & McLeod, B. 2010, ApJ, 708, 411

Kilic, M., Stanek, K. Z., & Pinsonneault, M. H. 2007, ApJ, 671, 761

Kurtz, M. J. & Mink, D. J. 1998, PASP, 110, 934

Landau, L. D. & Lifshitz, E. M. 1958, The classical theory of fields (Pergamon Press)

Liebert, J., Bergeron, P., & Holberg, J. B. 2005, ApJS, 156, 47

Marsh, T. R. 1995, MNRAS, 275, L1

Marsh, T. R., Dhillon, V. S., & Duck, S. R. 1995, MNRAS, 275, 828

Massey, P. 1997, A User's Guide to CCD Reductions with IRAF, National Optical Astronomy Observatory

Maxted, P. F. L., Marsh, T. R., & Moran, C. K. J. 2000, MNRAS, 319, 305

Morales, J. C. et al. 2009, ApJ, 691, 1400

Morales-Rueda, L., Marsh, T. R., Maxted, P. F. L., Nelemans, G., Karl, C., Napiwotzki, R., & Moran, C. K. J. 2005, MNRAS, 359, 648

Napiwotzki, R., Karl, C. A., Lisker, T., Heber, U., Christlieb, N., Reimers, D., Nelemans, G., & Homeier, D. 2004, Ap&SS, 291, 321

Nelemans, G. 2010, Ap&SS, 164

Nelemans, G. & Tauris, T. M. 1998, A&A, 335, L85

Nelemans, G. & Tout, C. A. 2005, MNRAS, 356, 753

Nelemans, G. et al. 2005, A&A, 440, 1087

Orosz, J. A., Wade, R. A., Harlow, J. J. B., Thorstensen, J. R., Taylor, C. J., & Eracleous, M. 1999, AJ, 117, 1598

Pickles, A. J. 1998, PASP, 110, 863

Postnov, K. & Yungelson, L. 2005, Living Rev. Rel., 9, 6

Press, W. 1994, Numerical Recipes in C (Cambridge: Cambridge University Press)

Rebassa-Mansergas, A., Nebot Gomez-Moran, A., Schreiber, M., Girven, J., & Gansicke, B. 2011, MNRAS, accepted

Reid, I. N., Turner, E. L., Turnbull, M. C., Mountain, M., & Valenti, J. A. 2007, ApJ, 665, 767

TABLE 2
BINARY ORBITAL PARAMETERS

Object	P (d)	K (km/s)	γ (km/s)	T_0 (days + 2450000)	F-Test	MF ($M_\odot$)	M_2 ($M_\odot$)	τ (Gyr)	No
PG 0132+254	. . .	(22)	17	. . .	No detectable period	. . .	. . .	. . .	1
PG 0237+242	0.7417±0.0269	78±9	−14±4	4386.6917±0.0154	$7.00e-06$	0.0371±0.0134	≥ 0.25	≤ 190	2
PG 0808+595	. . .	21±7	28±3	. . .	$7.16e-02$	. . .	. . .	. . .	1
PG 0834+501	1.2849±0.0564	58±9	−13±5	4464.0581±0.0441	$1.47e-05$	0.0262±0.0132	≥ 0.22	≤ 920	
PG 0846+249	. . .	(91)	−35	. . .	High dispersion	. . .	. . .	. . .	4
PG 0934+338	1.1142±0.0055	111±17	14±10	4465.7829±0.0205	$5.71e-07$	0.1604±0.0759	≥ 0.50	≤ 320	
PG 0943+441	. . .	(20)	49	. . .	No detectable period	. . .	. . .	. . .	1
PG 1022+050[a]	1.157±0.001	75±1	39±1	. . .	. . .	0.0500±0.0020	≥ 0.30	≤ 480	
PG 1036+086	1.3283±0.0109	83±18	93±11	4474.7431±0.0499	$1.55e-04$	0.0815±0.0525	≥ 0.37	≤ 610	
PG 1101+364[b]	0.145±0.001	71±2	39±1	. . .	. . .	. . .	0.37	2	4
PG 1114+224	0.3198±0.0147	34±7	44±3	4476.7679±0.0113	$1.46e-03$	0.0014±0.0009	≥ 0.07	≤ 64	
PG 1202+608[c]	1.493±0.001	77±8	0±6	. . .	. . .	0.0720±0.0200	≥ 0.34	≤ 93	
PG 1210+141[d]	0.642±0.001	131±3	15±2	. . .	. . .	0.1490±0.0100	≥ 0.46	≤ 90	
PG 1224+309[e]	0.260±0.001	112±14	−4±12	. . .	. . .	0.0380±0.0040	0.28	≤ 10	2
PG 1229−013	. . .	22±7	22±4	. . .	$2.48e-02$	. . .	. . .	. . .	1
PG 1241−010[f]	3.347±0.001	68±1	16±1	. . .	. . .	0.1110±0.0050	≥ 0.42	≤ 6700	
PG 1249+160	. . .	(16)	1	. . .	No detectable period	. . .	. . .	. . .	1
PG 1252+378	. . .	30±8	26±4	. . .	$3.00e-02$	. . .	. . .	. . .	2
PG 1317+453[f]	4.872±0.001	64±1	−24±1	. . .	. . .	0.1320±0.0040	≥ 0.44	≤ 19000	
PG 1320+645	. . .	(110)	−16	. . .	High dispersion	. . .	. . .	. . .	3
PG 1415+133	. . .	20±8	62±4	. . .	$7.97e-02$	. . .	. . .	. . .	2
PG 1458+172	0.1653±0.0003	143±8	73±12	4911.8550±0.0002	$1.08e-04$	0.1805	0.55	≤ 1.7	2,3
PG 1458 (Mg)	0.1653±0.0003	106±14	13±22	4913.7613±0.0003	$6.74e-03$	(0.0386)	(0.21)	(≤ 5.3)	
PG 1519+500	0.8603±0.0200	45±9	−31±4	4270.1663±0.0636	$8.90e-04$	0.0085±0.0051	≥ 0.14	≤ 460	
PG 1554+262	. . .	39±10	0±5	. . .	$1.58e-02$	. . .	. . .	. . .	1
PG 1614+136	. . .	25±6	-7±3	. . .	$1.44e-02$	. . .	. . .	. . .	1
PG 1654+637	. . .	25±9	29±4	. . .	$4.63e-02$	. . .	. . .	. . .	1
PG 1713+333[f]	1.127±0.001	56±1	56±1	. . .	. . .	0.0200±0.0010	≥ 0.19	≤ 700	
PG 2226+061	. . .	(23)	31	. . .	No detectable period	. . .	. . .	. . .	1
PG 2257+162	. . .	27±7	25±3	. . .	$2.30e-02$	. . .	. . .	. . .	2
PG 2331+290[f]	0.166±0.001	156±3	−11±3	. . .	. . .	0.0660±0.0040	≥ 0.34	≤ 2	

REFERENCES. — (a) Morales-Rueda et al. (2005), (b) Marsh (1995), (c) Holberg et al. (1995), (d) Nelemans et al. (2005), (e) Orosz et al. (1999), (f) Marsh e (1995)

NOTE. — (1) Probable single WD. (2) Infrared color excess, M dwarf companion. (3) Velocity variable, unconstrained orbit. (4) Double-lined spectroscopic bir